Classification System based on New Pathological Features for Diagnosing Stages of BilIN

JaeWon Song and JuHong Lee

Dept. of Computer Science & Information Technology, Inha University, Korea
sjw@datamining.inha.ac.kr, juhong@inha.ac.kr

Abstract

BilIN (Biliary INtraepithelial Neoplasm) is a precursor lesion of Intrahepatic CholangioCarcinoma (ICC). It is important to diagnose ICC and distinguish its stages for the prevention of ICC and proper treatment for a patient. BilIN is classified into BilIN-1, BilIN-2, and BilIN-3 by the morphological change and loss of polarity of epithelial cell and the structural abnormality of epithelium. This paper proposes two quantitative features based pathological knowledge for distinguishing stages of BilIN. The first feature is LumenBoundaryAbnomality (LBA) to measure the abnormal structure of epithelium; the second feature is NucleiPolarity for determine loss of polarity of epithelial cells. The experiment performed the stage classification of BilIN using following features; non-epithelial nuclei features, epithelial nuclei features, proposed features, non-epithelial nuclei and proposed features, epithelial nuclei and proposed features. The classification learning algorithm is used back-propagation Artificial Neural Networks. The classification result showed classification accuracies of 35% with non-epithelial features, 40% with epithelial features, 74% with proposed features, and 35% with non-epithelial and proposed features, and 46% with epithelial and proposed features.

Keywords: *BilIN, ICC, Nuclei Polarity, Lumen Boundary Abnormality, ANN*

1. Introduction

In Korea, after the hepatocellular carcinoma, ICC account for 5~10% of overall liver cancers as primary cancer. The only way to improve the survival rate of ICC patients is known as a radical excision [1]. But unfortunately, the radical excision of ICC is performed at only 30~50% of all ICC patients [2, 3]. The early detection of ICC is difficult, because initial symptom for ICC is rarely identified before it advances. Therefore, the detection of ICC at its early stages would increase survival possibility. Biliary Intraepithelial Neoplasia (BilIN) and Intraductal Papillary Neoplasm of bile duct (IPN) are known as precursors of ICC. So, the detection of these precursors and the classification of stages for them are very important for preventing progression into ICC and providing appropriate treatment to a patient. The BilIN is classified into BilIN-1, BilIN-2, and BilIN-3 by the atypia of cell, loss of nuclear polarity, and the change of epithelium architecture [4].

Especially, the stage grading of disease is an important work for a pathologist, because a prescription for a patient vary according to stages of disease [5]. Pathological diagnosis using the tissue of a patient is the most reliable diagnostic method. But, because the pathological diagnosis is performed through screening of tissue in high

magnification, the process is a time-consuming and requires enormous effort [5]. Also, the pathological diagnosis is very subjective, because it depends on experiences and knowledge of each individual doctor. However, the advent of the digital pathology equipment has made rapid and great advances in the pathological diagnosis that requires much time and work [6]. Now that the quantitative analysis and the rapid diagnosis are possible by using the digital image processing techniques for tissue slides that have been converted to digital image by digital pathology equipment.

This paper proposes a grading system based on Artificial Neural Network (ANN) for distinguishing stages of BilIN using the extracted morphological features from tissue image that is acquired through digital pathology equipment. The rest of the paper is organized as follows: Section 2 describes the pathological characteristics for distinguishing stages of BilIN; Section 3 talks about the proposed features for classifying the stages; Section 4 compares the experiment results for the existing features and the proposed features; and Section 5 presents our conclusions

2. Pathological Characteristics of BilIN

BilINs are characterized by atypical epithelial cells with multi-layer of nuclei and micropapillary projections into the duct lumen. The atypical cells have an increased nucleus-to-cytoplasm ratio, partial loss of nuclear polarity, and nuclear hyperchromasia. BilINs are separable into BilIN-1, BilIN-2, and BilIN-3 according to degree of atypia [7]. Table 1 describes the histopathological characteristics for classifying stages of BilIN.

Table 1. Pathological Characteristics for Classifying Stages of BilIN [4]

BilIN-1 (biliary intraepithelial neoplasia-1)
These lesions show flat or micropapillary architecture. Nuclei are basally located. Some lesions show focal nuclear pseudostratification; however, the nuclei remain within the lower two thirds of the epithelium. Cytologically, mild nuclear abnormalities, such as subtle irregularities of nuclear membrane, high nuclear/cytoplasmic ratios and nuclear elongation are seen. Nuclear sizes and shapes are relatively uniform, and the presence of large nuclei suggest a diagnosis of BilIN-2 or BilIN-3.
BlIN-2 (biliary intraepithelial neoplasia-2)
These lesions show flat, pseudopapillary or micropapillary architecture. Loss of cellular polarity is easily found, but it is not a diffuse feature. Nuclear pseudostratification reaching the luminal surface is common. Cytologically, dysplastic nuclear changes, which include enlargement, hyperchromasia and irregular nuclear membrane, are evident. Some variations in nuclear sizes and shapes are seen. Peribiliary glands are sometimes involved (glandular involvement). Mitoses are rare.
BilIN-3 (biliary intraepithelial neoplasia-3)
These lesions usually show pseudopapillary or micropapillary architecture, and are only rarely flat. They cytologically resemble carcinoma, but invasion through the basement membrane is absent. Cellular polarity is diffusely and severely distorted with nuclei reaching and piling on the luminal surface. ‘Budding off’ of small clusters of epithelial cells into the lumen and cribriforming can be seen. Cytologically malignant features with severe nuclear membrane irregularities, hyperchromasia or abnormally large nuclei are typically noted. Mitoses can be observed. Peribiliary gland involvement is sometimes found.

Figure 1 shows tissue images for BilIN-1, BilIN-2, and BilIN-3.

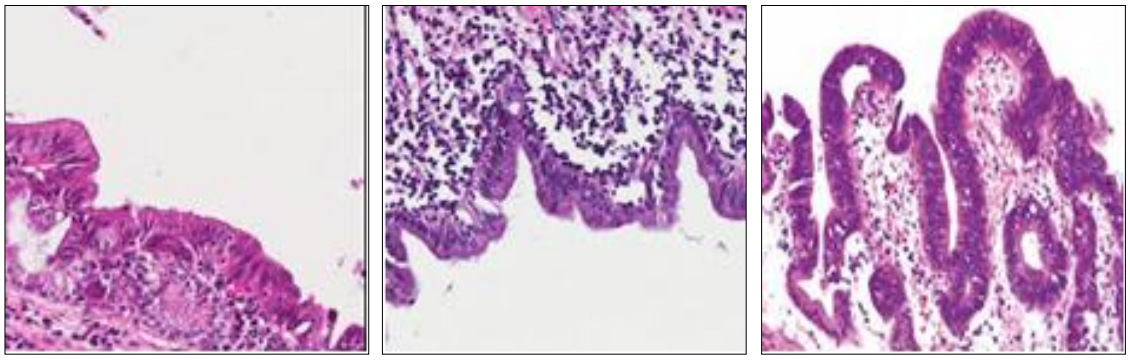

(a) (b) (c)

Figure 1. (a) Histological Picture of BilIN-1, (b) Histological Picture of BilIN-2, (c) Histological Picture of BilIN-3

Table 2 summarizes key characteristics of classifying the BilIN stages. In a single word, it is summarized that the BilIN stages are classified by the structural features of epithelium, loss of cellular polarity, and an atypia of epithelial nuclear.

Table 2. Major Summary for Grading Stages of BilIN

Type	Abnormality of epithelium Structure	Loss of Cellular Polarity	Atypia of Epithelial Nuclear
BilIN-1	flat or micropapillary architecture	Rare	Nuclear sizes and shapes are relatively uniform.
BilIN-2	flat, pseudopapillary or micropapillary architecture	easily found	Nuclear sizes and shapes has some
BilIN-3	pseudopapillary or micropapillary architecture	diffusely and severely distorted	Hyperchromasia or abnormally large nuclei are typically noted.

3. The Proposed Method

In this section, we discuss methods of quantitatively measuring the summarized pathological characteristics in Section 2 to distinguish the BilIN stages. There are many conducted studies for extracting morphological features for nuclear of Table 2 [8-10].Therefore, we use the methods that are proposed in [8-10] for extracting nuclear features. This paper focuses on the methods which measure the epithelium structure and the loss of polarity except for nuclear feature of Table 2.

3.1. Normal Lumen Boundary (NLB) Model and Lumen Boundary Abnormality

Firstly, we estimate the Normal Lumen Boundary (NLB) model from the given image tissue images in order to extract structural feature of epithelium. Generally, the lumen boundary of normal interahepatic bile duct is flat. But, according to progress stages of BilIN, the lumen boundary of the duct show papillary architecture. Therefore, from this fact, the normal lumen boundary can be assumed from lumen boundary of the given

intrahepatic bile duct. That is, the lumen boundary of a normal intrahepatic bile duct can be projected by generating linear model from the lumen boundary of given image.

The first step for generating NLB model is to detect a lumen boundary of given image. The lumen having white color can be easily identified by the *region-growing* algorithm [11] because it is adjacent to the epithelial cells. The identified lumen boundary by region growing method is denoted by B_L. Now, the NLB Model can be generated by using the identified lumen boundary B_L. As discussed above, if the given tissue image is normal, the lumen boundary is shown as a straight line. Thus, a point of the normal lumen boundary will appear the linear relationship at *x*-*y* coordinate system for the given tissue image. Therefore if we firstly assume that the coordinates, x and y, of points making up the lumen boundary have linear relationship, the NLB model can be represented as a simple linear equation.

$$y = \beta_0 + \beta_1 x + \varepsilon_i \tag{1}$$

Where, β_0 and β_1 represent the intercept and the slope respectively as unknown parameters to determine the linear equation of the lumen boundary. ε_i represents the model error. Then, if it is assumed that the ε_i are random variables with mean zero and constant variance σ^2, y_i will be represented by sum of both a deterministic component explained by the model and a random error component inexplicable by the model.

Now that, the relationship between the coordinates, *x* and *y*, of a point in the lumen boundary is assumed as $y = \beta_0 + \beta_1 x$ called the population NLB model. Then, the population parameters, β_0 and β_1, for determining the NLB model are estimated by the points, (x_1, y_1), …, (x_n, y_n) for lumen boundary. The Least Square Estimation (LSE) method is used to estimate the population parameters, β_0 and β_1, for the model. The LSE is the method to find the estimators $\hat{\beta}_0$ and $\hat{\beta}_1$ of β_0 and β_1 respectively that the residual sum of squares is minimized. Then, the estimated NLB model is defined as follows:

$$\hat{y} = \hat{\beta}_0 + \hat{\beta}_1 x \tag{2}$$

$$\hat{\beta}_1 = \frac{\sum_{i=1}^{m} (x_i - \bar{x})(\hat{y}_i - \bar{y})}{\sum_{i=1}^{n} (x_i - \bar{x})^2} \tag{3}$$

$$\hat{\beta}_0 = \bar{y} - \beta_1 \bar{x} \tag{4}$$

Here, *m* is the number of points in B_L, $\bar{y}$ is a mean of *y*, and $\hat{y}$ is the estimated response of the model.

Figure 2 (b) shows the estimated NLB model (red line) for Figure 2 (a). In Figure 2, the estimated population parameters, $\hat{\beta}_0$ and $\hat{\beta}_1$, are 584.064 and -0.237 respectively.

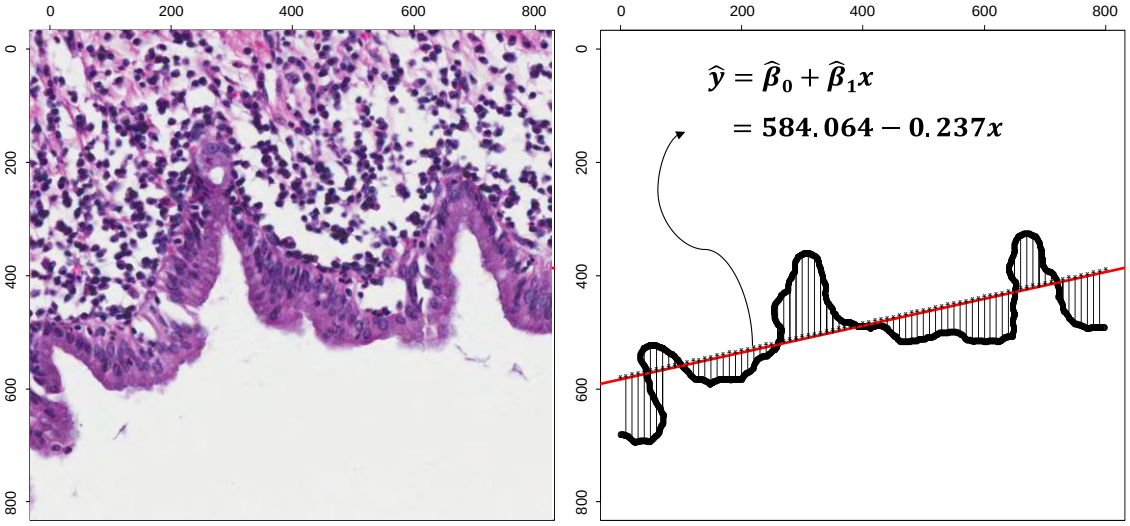

(a) (b)

Figure 2. (a) BilIN-2 with Abnormal Epithelium Architecture; (b) The Estimated NLB Model for (a)

The estimated NLB model is a linear relation for representing normal lumen boundary. Therefore, residual, e_i, between y_i in actual lumen point $p(x_i, y_i)$ and predicted $\hat{y}_i$ at xi means how far given lumen boundary is from normal boundary. The NLB model is based on the linear regression model in statistics. Therefore, the NLB model can use the statistics for the linear regression model.

We propose a feature for measuring the abnormal arrangement of lumen boundary using the NLB model. In regression analysis, the coefficient of determination R^2 is used to measure how well the estimated model performs as the predictors of observation y. R^2 is computed as SSR (regression sum of squares) divided by SST (Total sum of square).

$$R^2 = SSR / SST \tag{5}$$

$$SSR = \sum_{i=1}^{n} (\hat{y}_i - \bar{Y})^2 \tag{6}$$

$$SSE = \sum_{i=1}^{n} (Y_i - \hat{Y}_i)^2 \tag{7}$$

$$SST = \sum_{i=1}^{n} (Y_i - \bar{Y})^2 \tag{8}$$

Now, the abnormal arrangement of the lumen boundary that is denoted by *Lumen Boundary Abnormality* (*LBA)* is computed as the following equation by using the obtained coefficient of determination R^2.

$$LBA = 1 - R^2 \tag{9}$$

3.2. Cytoplasm Length and Nuclei Cellular Polarity

In this step, we discuss the method for measuring loss of cell polarity in epithelial cells. As mentioned in the Section 2, the loss of cellular polarity means that the epithelial nuclei are irregularly arranged due to the loos of nuclear polarity. In BilIN-1, the loss of cellular polarity in epithelium is rarely found. But, in advanced stages, BilIN-2 and BilIN-3, the loss of cellular polarity more easily is found. Figure 3 conceptually shows the case that the loss of polarity in epithelial cell does not appear and the case that it appears.

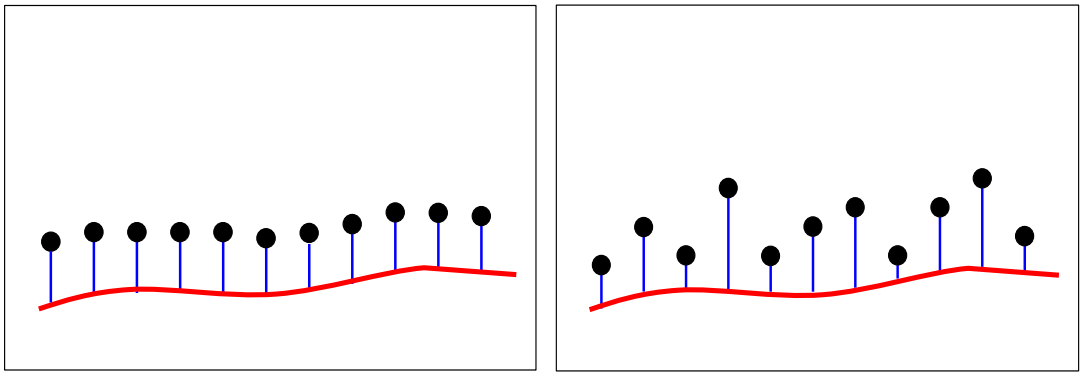

(a) (b)

Figure 3. Diagrams to Help Understanding for Loss of Polarity in Epithelial Cell; (a) The Case that Loss of Polarity in Epithelial Cells Does Not Occur; (b) The Case that Loss of Polarity in Epithelial Cells Occurs

In Figure 3, red line means lumen boundary, and black points represent epithelial nuclei surrounding the lumen. Blue line means the length of cytoplasm of epithelial cell. As shown Figure 3, if the occurrences of loss of cellular polarity appear, epithelial nuclei appear irregularly arranged. Therefore, if the loss of cellular polarity in epithelial cells is rare, the standard deviation for the cytoplasm length of epithelial cells is low as well. In contrast, if the loss of cellular polarity more appears, the standard deviation will increase.

First, to measure cytoplasm length of epithelial cell, nuclei should be identified from a given tissue image. The process of nuclei identification requires following 4 steps: 1) noise elimination through median filter; 2) remove of unnecessary parts such as cytoplasm; 3) Filling holes of threshold nuclei by hole-filling algorithm [11]; and 4) Identification nuclei using Watershed algorithm [12]. Then, a set of nuclei obtained by these four steps is denoted by N. Since epithelial nuclei are adjacent to lumen boundary B_L, epithelial nuclei N_E is selected by Eq. 10.

$$N_E = \bigcup_{j=1}^{m} \left\{ n \middle| p_j \in B_L, \min_{n \in N} distance(centroid(n), p_j) \right\} \quad (10)$$

where m is the number of points in B_L. The distance(·,·) is a function to measure *Euclidean* distance between given two points. The centroid(·) is a function returning the center point of a given object. Then, a set of non-epithelial nuclei N_{NE} is defined by N - N_E.

The length of cytoplasm is defined as an orthogonal distance from the epithelial nuclei to the lumen boundary.

$$\begin{aligned} &CytoplasmLength(n_i) = distance(centroid(n_i), p_k) \\ &\text{such that } centroid(n_i) \perp p_k \text{ and } p_k \in B_L \end{aligned} \quad (11)$$

Where, n_i is an element of N_E. With this, Nuclei Polarity can be drawn by calculating the standard deviation of the cytoplasm lengths for epithelial nuclei.

$$NucleiPolarity = \sqrt{\frac{1}{m}\sum_{i=1}^{m}(CytoplasmLength(n_i) - mean_E} \quad (12)$$

Where, m implies cardinality of N_E. The $mean_E$ is the mean of *CytoplasmLength*s.

4. Experiment

4.1. Experiment Design

For the experiment, we received tissue samples from YeungNam University's Department of Pathology. The tissue samples used in experiment are stained by Hematoxylin & Eosin. The tissue slides were scanned into a digital image of 20x optical magnification using aperio's slide scanner equipment, "ScanScope CS System (www.aperio.com)". We converted each of 60 images including epithelium into a 512×512, 24bit tiff file for BilIN-1, BilIN-2, and BilIN-3.

Table 3 shows the number of slides and images that used in experiments.

Table 3. Experiment Data

Type	Number of slides	Number of experiment images
BilIN-1	3	60
BilIN-2	3	60
BilIN-3	3	60

The experiments are designed to classify 3 stages of BilIN using the existing nuclei features and the proposed *LBA* and *NucleiPolarity*. In this paper, nuclei are divided into non-epithelial nuclei and epithelial nuclei. So, we extracted features of nuclei of N_E and N_{NE} such as *area*, *perimeter*, *width*, *height*, *major axis*, *minor axis*, *angle*, *circularity*, *feret's diameter*, *feret's angle*, *skewness*, *aspect ratio*, *roundness*, and *solidity*. Refer to [8-10] for the detail

description of these features. The classifier to categorize stages of BilIN into BilIN-1, BilIN-2, and BilIN-3 is learned by back-propagation ANN.

In reality, the number of samples that can be obtained is very circumscribed, because the number of cases that is secured at a hospital is very small, and also the share of cases between hospitals is not active yet. Thus, we evaluated the classification performance using bootstrap method [13]. For the bootstrap evaluation, 10 training sets and 10 testing sets are generated through resampling from feature data. The ratio of training set to test set was 50 to 50. The final result for classification is measured by averaging results of 10 classifiers. The ANN is consisted of three layers (input-hidden-output). In each experiment, the optimal number of hidden nodes is determined as increasing number of hidden nodes from 5 ~ 20 and the performance of the classifier is evaluated. Then, the evaluation for selecting the number of optimal hidden nodes is conducted by 10-fold cross validation on training data.

The classification experiments are consisted of: 1) classification experiment using non-epithelial nuclei features; 2) classification experiment using epithelial nuclei features; 3) classification experiment using the proposed features (*LBA* and *NucleiPolarity*); 4) classification experiment using the non-epithelial nuclei and proposed features; and 5) classification experiment using the epithelial nuclei and proposed features.

4.2. Results and Discussion

Tables 4, 5, 6, 7 and 8 shows the experiment results that are conducted in this paper.

Table 4. Confusion Table with Non-epithelial Nuclei

		Predicted Class			Correct Classification (%)
		BilIN-1	**BilIN-2**	**BilIN-3**	
Actual Class	**BilIN-1** (*n*=30)	1.70	5.90	22.40	5.67
	BilIN-2 (*n*=30)	0.00	6.00	24.00	20.00
	BilIN-3 (*n*=30)	0.20	6.00	23.80	79.33
Total Accuracy					35.00

*where *n* is the number of test data.

Table 5. Confusion Table with Epithelial Nuclei

		Predicted Class			Correct Classification (%)
		BilIN-1	**BilIN-2**	**BilIN-3**	
Actual Class	**BilIN-1** (*n*=30)	10.90	3.50	15.60	36.33
	BilIN-2 (*n*=30)	5.50	2.80	21.70	9.33
	BilIN-3 (*n*=30)	4.50	3.10	22.40	74.67
Total Accuracy					40.11

Table 6. Confusion Table with the Proposed Features

		Predicted Class			Correct Classification (%)
		BilIN-1	BilIN-2	BilIN-3	
Actual Class	**BilIN-1** (*n*=30)	21.80	7.00	1.20	72.67
	BilIN-2 (*n*=30)	2.40	20.90	6.70	69.67
	BilIN-3 (*n*=30)	0.30	5.40	24.30	81.00
Total Accuracy					74.44

Table 7. Confusion Table with the Non-epithelial and the Proposed Features

		Predicted Class			Correct Classification (%)
		BilIN-1	BilIN-2	BilIN-3	
Actual Class	**BilIN-1** (*n*=30)	1.70	5.90	22.40	5.67
	BilIN-2 (*n*=30)	0.00	6.00	24.00	20.00
	BilIN-3 (*n*=30)	0.20	6.00	23.80	79.33
Total Accuracy					35.00

Table 8. Confusion Table with the Epithelial and the Proposed Features

		Predicted Class			Correct Classification (%)
		BilIN-1	BilIN-2	BilIN-3	
Actual Class	**BilIN-1** (*n*=30)	13.80	11.20	5.00	46.00
	BilIN-2 (*n*=30)	3.70	19.00	7.30	63.33
	BilIN-3 (*n*=30)	2.10	18.90	9.00	30.00
Total Accuracy					46.44

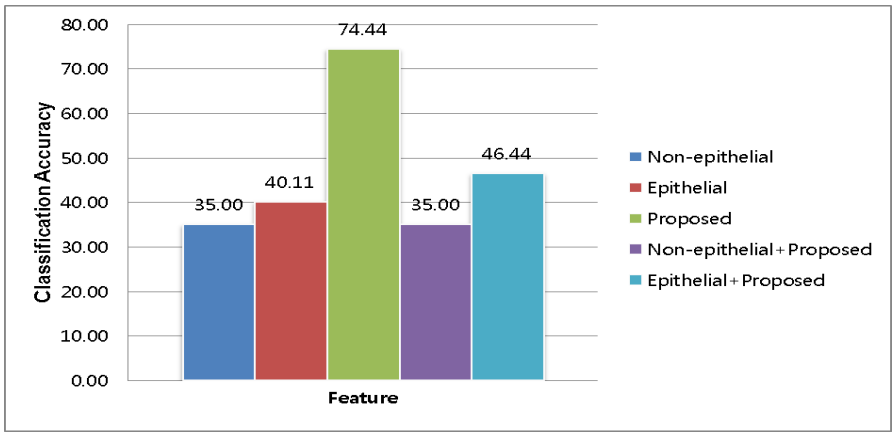

Figure 4. Classification Accuracy

The classification results show classification accuracies of 35%, 40%, and 74% in the classifiers with non-epithelial nuclei features, epithelial nuclei features, and proposed features respectively. The results explain that the proposed features are more suitable for the stage grading than non-epithelial nuclei and epithelial nuclei features. Especially, the experiment with non-epithelial nuclei features shows the lowest classification performance. It means that the epithelial cell and architecture of lesion features are more effective to distinguish stages of BilIN.

Next, we performed the experiment with non-epithelial nuclei and proposed features and the experiment with epithelial nuclei and features to examine how they improve classification performance through a feature combination. The results show in Table 7 and Table 8 respectively. In these two experiments, the classification accuracy is lower than one using only proposed features. That is, performance improvement of the classifier by combination of nuclei feature and nuclei features has not been proved.

Table. 9, 10, 11 show box plots of the non-epithelial nuclei, epithelial nuclei, and proposed features. Overall, in the epithelial nuclei and non-epithelial nuclei features, much overlap between stages of BilIN has appeared. In contrast, the box plot of proposed features showed lower overlap between the stages. It shows that in classifying between the stages why the performance of classifier with proposed feature is better than classifiers with either non-epithelial nuclei or epithelial nuclei feature.

Table 9. Box-plots of Non-epithelial Nuclei Features

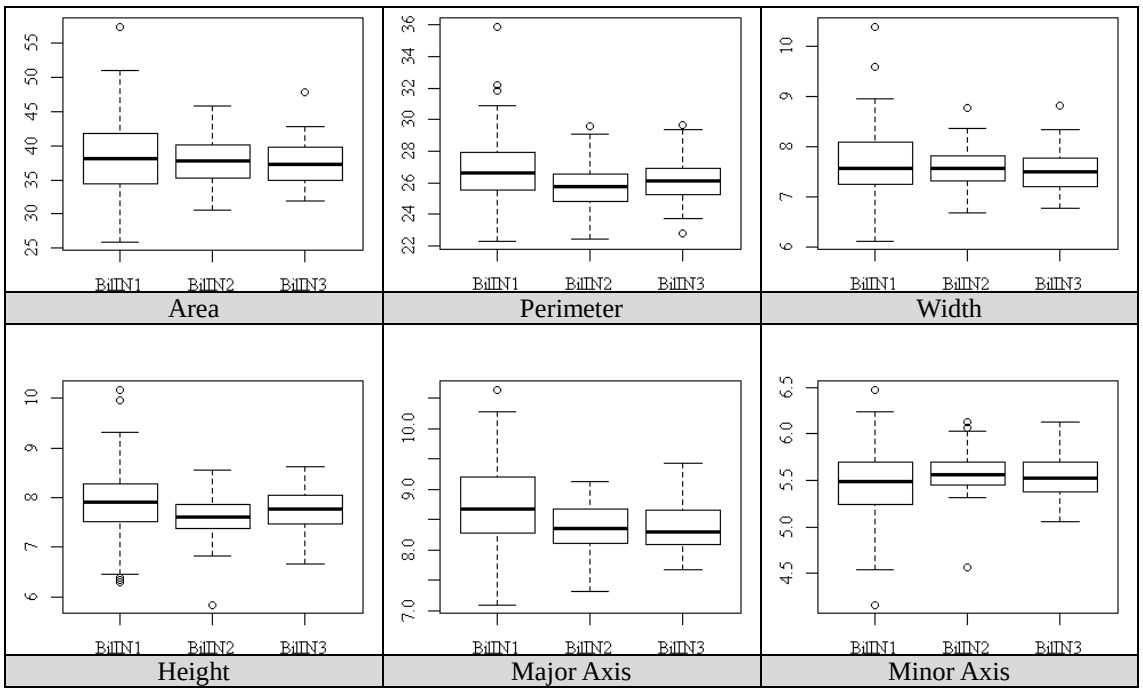

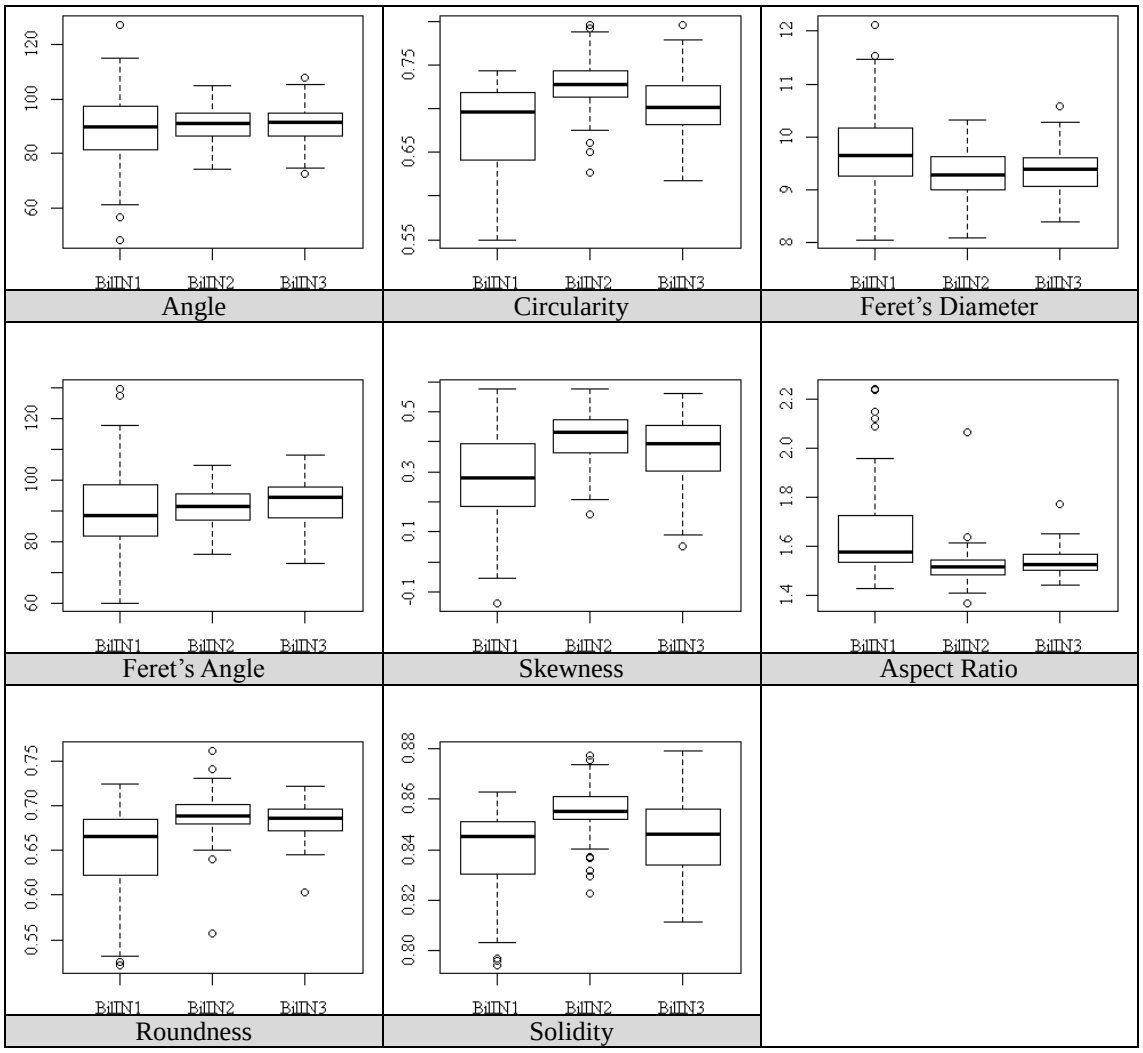

Table 10. Box-plots of Epithelial Nuclei Features

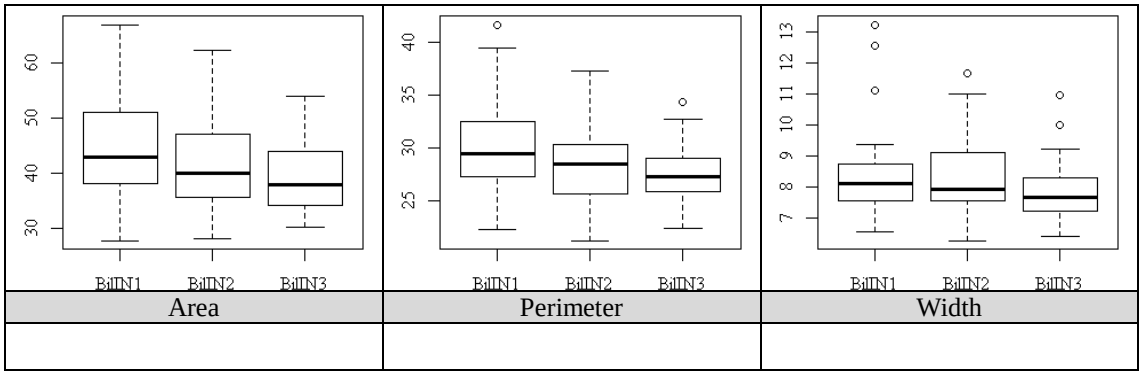

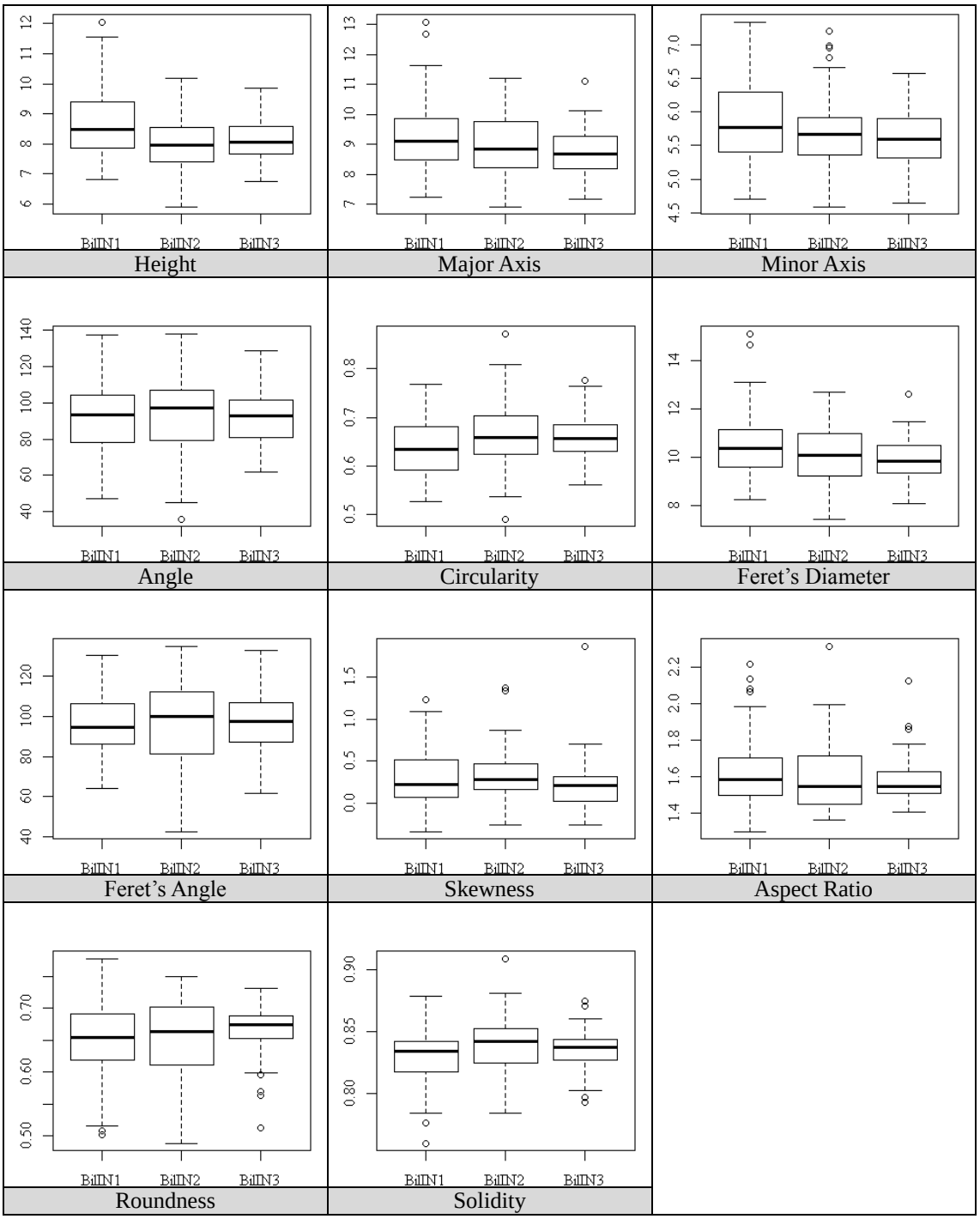
Height
Major Axis
Minor Axis
Angle
Circularity
Feret's Diameter
Feret's Angle
Skewness
Aspect Ratio
Roundness
Solidity
BiIIN1
BiIIN2
BiIIN3

Table 11. Box-plots of Proposed Features

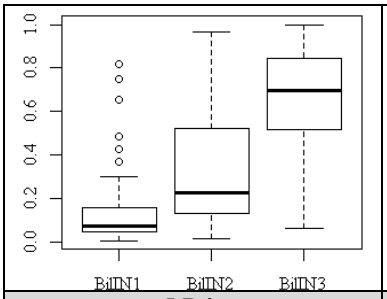	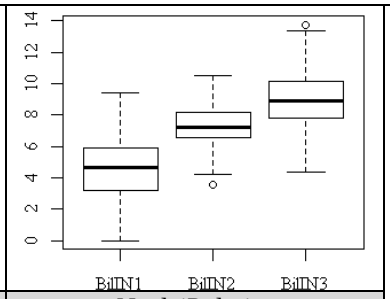	
LBA	NucleiPolarity	

5. Conclusion

The stages of BilINs are divided by the atypia of epithelial nuclei, the loss of polarity in epithelial cells, and the architecture of lesion. In this paper, we generated NLB model and proposed *LBA* feature for quantitatively measuring the structure of abnormal epithelium. Also, for measuring loss of polarity in epithelial cells, *NucleiPolarity* feature was extracted. For showing the superiority of the proposed features, the experiments compared classification performances of ANN classifiers that are individually leant by non-epithelial features, epithelial features, and proposed features. The experiment and the result analysis showed that the proposed features are suitable for classifying stages of BilIN.

Acknowledgements

This research was supported by Basic Science Research Program through the National Research Foundation of Korea (NRF) funded by the Ministry of Education, Science and Technology (2010-0024216).

References

[1] J. R. Eun, B. I. Jang, J. Y. Lee, K. O. Kim, S. H. Lee, T. N. Kim and H. J. Lee, "Clinical characteristics of intrahepatic cholangiocarcinoma and prognostic factors in patients who received non-surgical treatment", Korean J Gastroenterol, vol. 54, no. 4, **(2009)** October, pp. 227–234.
[2] W. J. Lee and J. W. Park, "Review: analysis of survival rate and prognostic factors of intrahepatic cholangiocarcinoma: 318 cases in single institute", Korean J Hepatol, vol. 13, no. 2, **(2007)** June, pp. 125–128.
[3] M. F. Chen, Y. Y. Jan, L. B. Jeng, T. L. Hwang, C. S. Wang, S. C. Chen, T. C. Chao, H. M. Chen, W. C. Lee, T. S. Yeh and Y. F. Lo, "Intrahepatic cholangiocarcinoma in Taiwan", J Hepatobiliary Pancreat Surg, vol. 6, no. 2, **(1999)**, pp. 136–141.
[4] Y. Zen, N. V. Adsay, K. Bardadin, R. Colombari, L. Ferrell, H. Haga, S. -M. Hong, P. Hytiroglou, G. Klöppel, G. Y. Lauwers, D. J. van Leeuwen, K. Notohara, K. Oshima, A. Quaglia, M. Sasaki, F. Sessa, A. Suriawinata, W. Tsui, Y. Atomi and Y. Nakanuma, "Biliary intraepithelial neoplasia: an international interobserver agreement study and proposal for diagnostic criteria", Mod. Pathol., vol. 20, no. 6, **(2007)** June, pp. 701–709.
[5] M. N. Gurcan, L. E. Boucheron, A. Can, A. Madabhushi, N. M. Rajpoot and B. Yener, "Histopathological Image Analysis: A Review", IEEE Reviews in Biomedical Engineering, vol. 2, **(2009)**, pp. 147 –171.
[6] S. J. Potts, "Digital pathology in drug discovery and development: multisite integration", Drug Discov. Today, vol. 14, no. 19–20, **(2009)** October, pp. 935–941.

[7] Y. Nakanuma, M. -P. Curado, S. Franceschi, G. Gores, V. Paradis, B. Sripa, W. M. S. Tsui and A. Wee, “Intrahepatic cholangiocarcinoma”, in WHO Classification of Tumours of the Digestive System, 4th ed., vol. 3, International Agency for Research on Cancer, **(2010)**, pp. 217–224.
[8] T. Allen, "Particle Size Measurement", vol. 1, Powder sampling and particle size measurement, Springer, **(1996)**.
[9] W. N. Street, W. H. Wolberg and O. L. Mangasarian, “Nuclear feature extraction for breast tumor diagnosis”, in Society of Photo-Optical Instrumentation Engineers (SPIE) Conference Series, vol. 1905, **(1993)**, pp. 861–870.
[10] C. Demir and B. Yener, “Automated Cancer Diagnosis Based on Histopathological Systematic Images: A Systematic Survey”, Rensselaer Polytechnic Institute, **(2005)**.
[11] R. C. Gonz á lez and R. E. Woods, "Digital Image Processing", Prentice Hall, **(2008)**.
[12] C. Pan, C. -X. Zheng and H. -J. Wang, “Robust color image segmentation based on mean shift and marker-controlled watershed algorithm”, in 2003 International Conference on Machine Learning and Cybernetics, vol. 5, **(2003)**, pp. 2752 – 2756.
[13] B. Efron and R. Tibshirani, "An Introduction to the Bootstrap (Chapman & Hall/CRC Monographs on Statistics & Applied Probability", Chapman and Hall/CRC, **(1994)**.

Authors

Jae-Won Song is currently a Ph.D. candidate in Dept. of Computer and Information Engineering at Inha University. He received a M.S. degree in Dept. of Computer and Information Engineering from the Inha University of South Korea in 2007. His research interests include data mining, ontology and medical image processing.

Ju-Hong Lee received the B.S. and M.S. in Dept. of Computer Engineering from Seoul National University in 1983 and 1985, and the Ph.D. from Korea Advanced Institute of Science and Technology in 2001. He is currently a Professor of Dept. of Computer and Information Engineering at Inha University. His research interests include data mining, information retrieval, and medical image processing.